Journal of Volcanology and Geothermal Research 357 (2018) 152–162

Contents lists available at ScienceDirect

Journal of Volcanology and Geothermal Research

journal homepage: www.elsevier.com/locate/jvolgeores

Investigating collapse structures in oceanic islands using magnetotelluric surveys: The case of Fogo Island in Cape Verde

F.J. Martínez-Moreno [a,*], F.A. Monteiro Santos [a], J. Madeira [a], J. Pous [b], I. Bernardo [a], A. Soares [a], M. Esteves [a], F. Adão [a], J. Ribeiro [a], J. Mata [a], A. Brum da Silveira [a]

[a] Instituto Dom Luiz, Faculdade de Ciências, Universidade de Lisboa, 1749-016 Lisboa, Portugal
[b] Departament de Dinàmica de la Terra i l'Oceà, Facultat de Ciències de la Terra, Universitat de Barcelona, C/Martí i Franquès s/n., 08028 Barcelona, Spain

ARTICLE INFO

Article history:
Received 13 September 2017
Received in revised form 17 April 2018
Accepted 25 April 2018
Available online 30 April 2018

Keywords:
Volcanic ocean islands
Magnetotelluric
Flank collapse
Island structure
Resistivity

ABSTRACT

One of the most remarkable natural events on Earth are the large lateral flank collapses of oceanic volcanoes, involving volumes of rock exceeding tens of km^3. These collapses are relatively frequent in recent geological times as supported by evidence found in the geomorphology of volcanic island edifices and associated debris flows deposited on the proximal ocean floor. The Island of Fogo in the Cape Verde archipelago is one of the most active and prominent oceanic volcanoes on Earth. The island has an average diameter of 25 km and reaches a maximum elevation of 2829 m above sea level (m a.s.l.) at Pico do Fogo, a young stratovolcano located within a summit depression open eastward due to a large lateral flank collapse. The sudden collapse of the eastern flank of Fogo Island produced a megatsunami ~73 ky ago. The limits of the flank collapse were deduced as well from geomorphologic markers within the island. The headwall of the collapse scar is interpreted as either being located beneath the post-collapse volcanic infill of the summit depression or located further west, corresponding to the Bordeira wall that partially surrounds it. The magnetotelluric (MT) method provides a depth distribution of the ground resistivity obtained by the simultaneous measurement of the natural variations of the electric and magnetic field of the Earth. Two N-S magnetotelluric profiles were acquired across the collapsed area to determine its geometry and boundaries. The acquired MT data allowed the determination of the limits of the collapsed area more accurately as well as its morphology at depth and thickness of the post-collapse infill. According to the newly obtained MT data and the bathymetry of the eastern submarine flank of Fogo, the volume involved in the flank collapse is estimated in ~110 km^3. This volume –the first calculated onshore– stands between the previously published more conservative and excessive calculations –offshore– that were exclusively based in geomorphic evidence. The model for the summit depression proposing two caldera collapses preceding the collapse of the eastern flank of Fogo is supported by the MT data.

1. Introduction

Volcanic edifices become progressively unstable as they grow and, therefore, large volcanoes may suffer swift large-scale geomorphological changes produced by collapse processes. These major volcanotectonic events include gravitational caldera vertical collapses and lateral flank collapses that occur periodically during the evolution of large volcanoes (Merle and Lénat, 2003). Vertical collapses of caldera type, truncating the volcano summit, are common in the evolution of large volcanoes due to a deficit of mass in depth (magma reservoirs) as a consequence of magma transfer. Lateral flank collapses may occur when the volcanic structure becomes gravitationally unstable, a process enhanced by the island geological structure, which is usually characterized by seawards dipping layers of alternating coherent and incoherent volcanic and sedimentary deposits.

Large lateral flank collapses in oceanic volcanoes, involving volumes exceeding tens of km^3, are one of the most remarkable natural events on Earth (Ward and Day, 2001). Although no such event has been observed in historical times, their evidence in the geomorphology of volcanic island edifices and from the associated debris flows and turbidites deposited on the surrounding ocean floor indicate their relatively frequent occurrence in recent geological times. Numerous examples of lateral collapses have been described in most volcanic archipelagos. As examples we mention Cape Verde (Day et al., 1999; Amelung and Day, 2001; Masson et al., 2008; Madeira et al., 2008; Ramalho et al., 2015); Canaries (Watts and Masson, 1995; Masson, 1996; Day, 2001; Masson et al., 2002; Carracedo, 2014), Hawaii (Morgan et al., 2003; Coombs et al., 2004; Okubo, 2004); Stromboli in the Aeolian Islands (Tibaldi, 2001; Acocella and Tibaldi, 2005; Vezzoli and Corazzato, 2016); Ritter Island in Papua-New Guinea (Ward and Day, 2003; Day et al., 2015);

* Corresponding author.
E-mail address: fjmoreno@fc.ul.pt (F.J. Martínez-Moreno).

https://doi.org/10.1016/j.jvolgeores.2018.04.028
0377-0273/

Reunion Island (Oehler et al., 2008). This type of events is also reported in continental volcanoes such as the 7200 years BP Socompa flank collapse in the Andes (De Silva and Francis, 1991) or Colima in México (Cortés et al., 2010), among others.

Growing instability as volcanoes become taller and steeper may originate failures of variable scale, ranging from minor rock falls to giant megaslides involving volumes of rock of the order of tens to hundreds of km^3 (McGuire, 1996). Generally, major structural failure is limited to the larger volcanic edifices. Persistent dyke emplacement producing rifting and generating local seismicity, deformation and changes in edifice pore-pressure, together with environmental factors, constitute potential failure triggers. In addition, ground deformation induced by magma injection and ground shaking caused by tectonic earthquakes and/or surface fault rupture may contribute in the instability of the volcanic edifices. Other processes that can activate a lateral collapse are: asymmetric distribution of buttressed flanks (Romagnoli et al., 1993; Romagnoli and Tibaldi, 1994), glacio-eustatic sea-level variations (Della Seta et al., 2013; Lee, 2009), slope erosion by marine abrasion on littoral areas (Tibaldi et al., 1994; Ramalho et al., 2013) and hydrothermal alteration in the core of volcanoes (López and Williams, 1993; Day, 1996; Voight and Elsworth, 1997; Martí et al., 1997; Van Wyk de Vries et al., 2000; Reid et al., 2001; Ferrer et al., 2010; Merle et al., 2010).

The Island of Fogo in the Cape Verde archipelago (Fig. 1a) is a very active and prominent oceanic volcano (Ribeiro, 1960). The island has an average diameter of 25 km and reaches a maximum elevation of 2829 m above sea level (m a.s.l.) at Pico do Fogo, a young stratovolcano located within a summit depression open eastwards due to a large lateral flank collapse (Brum da Silveira et al., 1997; Day et al., 1999; Paris et al., 2011; Le Bas et al., 2007; Madeira et al., 2008; Masson et al., 2008). The lateral limits of the flank collapse in Fogo can be deduced from geomorphological markers, namely the 400 m tall Espigão escarpment marking its southern lateral limit and a more subdued escarpment, partially covered by recent volcanic deposits, at its northern edge. The headwall of the flank collapse scar is interpreted as either being located beneath the post-collapse volcanic infill of the summit depression (Brum da Silveira et al., 1997; Torres et al., 1998) or located further west, corresponding to the Bordeira wall (Fig. 1) that partially surrounds the summit depression (Day et al., 1999). There are two genetic interpretations for the summit depression. According to Brum da Silveira et al. (1997), Torres et al. (1998) and Madeira et al. (2008), it is the result of two caldera collapses: an older southern caldera, 6 km in diameter, and a younger and smaller northern one, 3.5 km in diameter, whose floor lies approximately 50 m lower than the southern caldera. The intersection of the two calderas forms the Monte Amarelo spur (Fig. 1b). According to these authors the summit caldera depression was opened to the east by a large flank collapse. Another interpretation is presented by Day et al. (1999) that consider the whole depression as being produced by a large collapse of the eastern flank of the volcano, with the Bordeira corresponding to its headwall (Fig. 1c). Most subsequent works follow the later interpretation (i.e. Masson et al., 2008; Paris et al., 2011; Maccaferri et al., 2017). These two alternative interpretations have important consequences in terms of area and volume of the flank collapse and in understanding the evolution of the island. Besides the uncertainty on the surface trace of the collapse scar, the calculation of the volume involved depends also on the volcano morphology prior to the flank collapse and the depth of the rupture surface which was unknown until now. The geology and geomorphology show that it lies below sea-level at the island eastern seaboard, but its depth inland was still unknown. This problem can only be addressed by drilling or by geophysical methods.

Our work aims at defining the geometry of the lateral flank collapse in Fogo Island and, if possible, to choose between the two competing models for the collapse structure by means of the magnetotelluric (MT) method. MT data can provide depth distribution of the ground resistivity obtained by simultaneous measurement of the natural variations of the electric and magnetic field of the Earth (Vozoff, 1991). This method allows obtaining profile or map resistivity distributions down to depths of thousands of meters thus having the potential to image collapse scars in depth. Two profiles crossing the collapsed area, either caldera and/or flank collapses, were used to determine the geometry of Fogo collapse structures both at the surface and at depth, and thus estimating the area and volume involved.

2. Geological setting

Cape Verde Archipelago, located 570 km off the west coast of Africa, is formed by ten major islands (Fig. 2a) displaying a horseshoe shape open to the west. The islands are built on Late Jurassic to Cretaceous oceanic crust on top of a major topographic anomaly – the Cape Verde Rise. The magmatism is considered to be the result of a mantle plume (White, 1989) and the ages of the oldest subaerial lavas suggest that the islands emerged during the Miocene (Mitchell et al., 1983; Torres et al., 2002; Plesner et al., 2003; Duprat et al., 2007; Holm et al., 2008; Madeira et al., 2010; Dyhr and Holm, 2010; Ramalho et al., 2010; Ancochea et al., 2010, 2014 and 2015). The morphology of the islands is related to their age, so that the westernmost younger islands (Brava, Fogo, Santiago, São Nicolau, Santa Luzia, São Vicente, Santo Antão) present

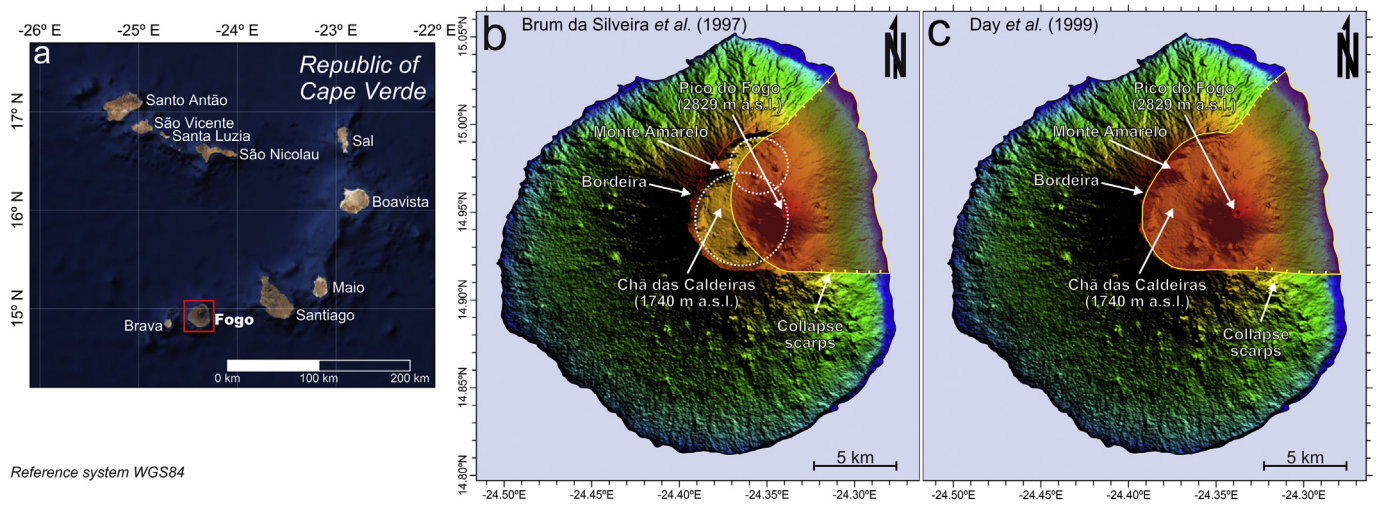

Fig. 1. Geographical location of the island of Fogo in Cape Verde archipelago (a). Models proposed for the origin of the Bordeira wall: (b) a combination of two caldera collapses followed by a flank collapse (Brum da Silveira et al., 1997) and (c) a single major collapse of the eastern flank of the volcanic edifice (Day et al., 1999). Modified from Ramalho et al., 2015.

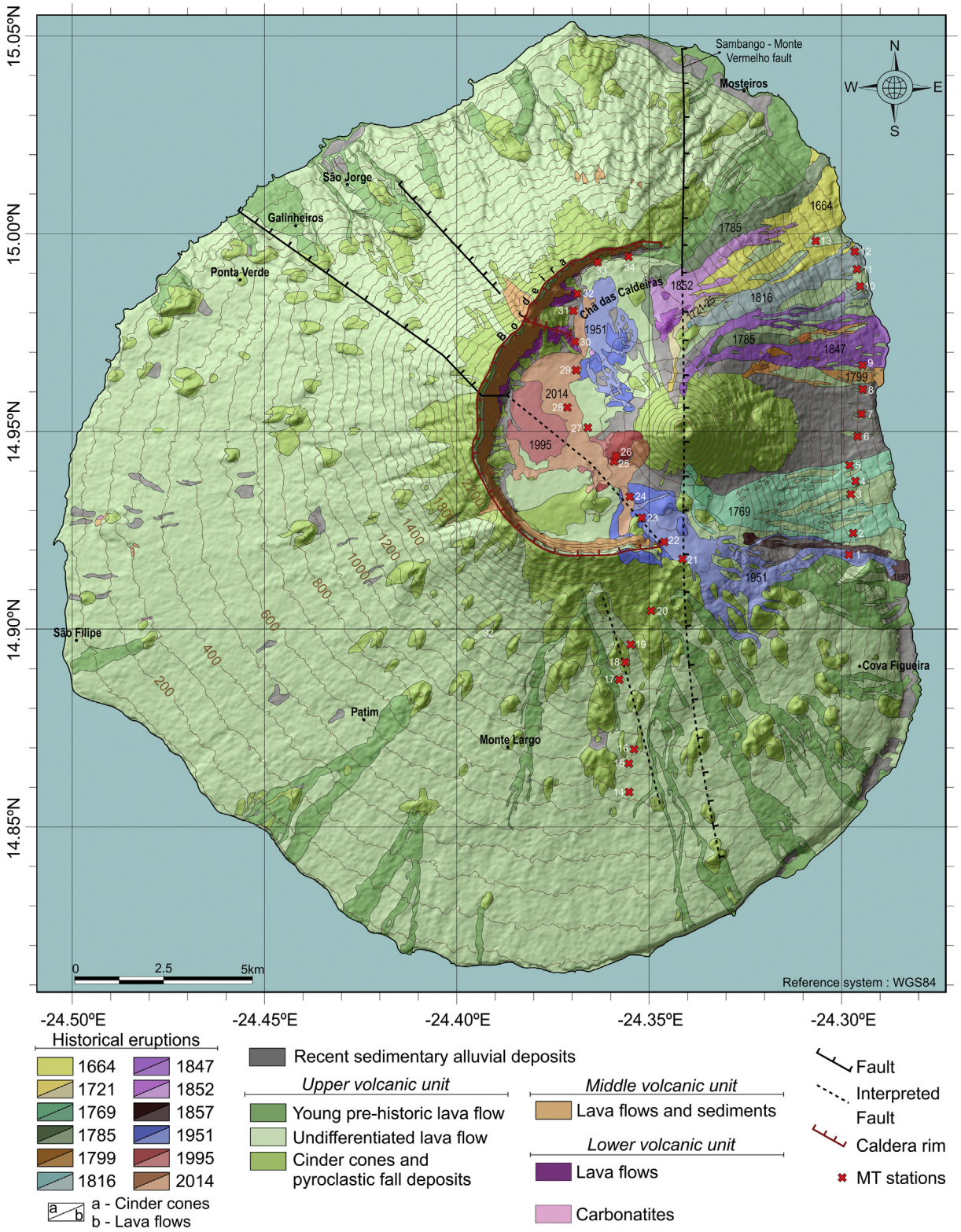

Fig. 2. Geological map of the island (Modified from Torres et al., 1998). The red crosses indicate the location of the magnetotelluric stations. (For interpretation of the references to colour in this figure legend, the reader is referred to the web version of this article.)

vigorous morphologies that contrasts with the razed topography of the easternmost older islands (Sal, Boavista and Maio).

The island of Fogo is located on the southern arm of the U-shaped archipelago. Fogo is the fourth largest island in Cape Verde with a surface area of 476 km^2, culminating at 2829 m a.s.l. at Pico do Fogo which represents the highest elevation in the archipelago. The island is formed by a major conical and asymmetrical Quaternary strato-volcano (Fig. 2). The morphological asymmetry is mainly the result of the dominant north-easterly trade winds. Most precipitation falls on the windward flank and thus the slopes are steeper and the radial stream network

more incised (Martínez-Moreno et al., 2016). The north littoral is also characterized by taller sea cliffs as a result of more intense wave abrasion produced by the dominant wave regime.

Fogo is mostly formed of basanitic lava flow piles with minor intercalations of pyroclastic and sedimentary layers. A small outcrop of an older (Pliocene) basement formed by intrusive carbonatites (Hoernle et al., 2002) covered by lava flows from younger volcanic units lies 3 km to the N of the São Filipe city. Fogo is the only capeverdian island presenting post-settlement volcanism, with references to at least 27 eruptions since the mid-15th century (Ribeiro, 1960). The latest Fogo eruption started on November 23rd, 2014 and lasted until early February 2015 (Bagnardi et al., 2016; Cappello et al., 2016; Richter et al., 2016; Mata et al., 2017). The summit of the volcano is truncated by an 8 km-wide depression (Chã das Caldeiras; Fig. 2b) open to the E and surrounded on the other sides by the Bordeira, an almost vertical wall reaching a maximum height of 1000 m, (Fig. 3). The 1100 m-tall young cone of Pico do Fogo grew on the summit depression (Fig. 2b). The outer slopes of Fogo are covered by pre-historical lava flows issued from parasitic cones, aligned on radial and concentric feeder dikes, extending from the rim of the summit depression down to sea level.

After the collapse event(s), the depression was totally covered and partially filled by pre-historical and historical lava flows and locally by lahars (Ribeiro, 1960; Torres et al., 1998). Besides the geomorphologic evidence, the flank collapse hypothesis is supported by the presence of submarine debris avalanche deposits that extend offshore to the E of the island, matching with the collapse scar (Masson et al., 2008). Madeira et al. (2008) present a conservative calculation of the removed rock volume of 70 km^3 using an area of 700 km^2 for the submarine debris avalanche according to the swath bathymetry published by Masson et al. (2008) and an average debris avalanche thickness of 100 m. According to Paris et al. (2011) and Ramalho et al. (2015), the massive flank originated a megatsunami that stroke the neighbouring island of Santiago. Ramalho et al. (2015) showed that the tsunami generated waves with minimum height of 170 m at the N coast of this island, with correlative tsunamigenic conglomerates being found as high as 100 m above present sea level (a.p.s.l.), while megaclasts plucked from the cliff edge were transported inland up to 220 m a.p.s.l. The age of deposition of the megaclasts was determined by cosmogenic exposure setting the probable age for the flank collapse at about 73 ky ago.

3. The Magnetotelluric method

The magnetotelluric (MT) method allows the estimation of resistivity distribution underground by measuring the natural variations of the surface electric (**E**) and magnetic fields (**H**) over a wide frequency range (e.g. Vozoff, 1991). The horizontal component of electric and magnetic fields is related as follow:

$$\mathbf{E} = \underline{Z}^{*}\mathbf{H} \tag{1}$$

where $\underline{Z}$ represent the 2×2 impedance tensor that describes the resistivity structure under the measuring site, and its off-diagonal components are used here to calculate the apparent resistivity functions (ρ_{xy} and ρ_{yx}) and the phase functions ($\varnothing xy$ and $\varnothing yx$) which are defined as:

$$\rho xy = 1/(\omega\mu_o)|Z_{xy}|^2 \tag{2}$$

$$\rho_{xy} = 1/(\omega\mu_o)\,|Z_{yx}|^2 \tag{3}$$

$$\varnothing xy = \arg(Zxy) \tag{4}$$

$$\varnothing yx = \arg(Zyx) \tag{5}$$

where ω represents the angular frequency and μ_o is the magnetic permeability.

Magnetotelluric data was acquired with the equipment ADU-07 Metronix system operated at a frequency range from 1000 Hz up to 1 Hz. The four components of the tensor were recorded being x North and y East. The distribution of the MT stations was organized along two roughly N-S profiles crossing the depressed area (Fig. 4) in accordance with the interpreted collapse and tectonic structures. Profile 1 includes 13 MT stations and was obtained along the E coast of the island. The average elevation goes from ~500 m a.s.l. at the S, to ~300 m a.s.l. at the N. Profile 2 comprises 21 MT stations crossing the summit depression. This profile presents wider topographic variation, ranging from ~550 m a.s.l. at mid-slope at the S to ~1800 m inside the summit depression.

3.1. Ocean effect and depth of resolution

Since the survey was carried out in an island it is important to study if the data are affected by the so-called 'ocean effect'. The distortion produced in MT measurements by the ocean depends on the distance from the coast, bathymetry and land resistivity distribution (Monteiro Santos et al., 2001, 2006; González-Castillo et al., 2015). In profile 1 the MT sites are located a few hundred meters away from the littoral, while profile 2 is located at ~5 km from the coast (Fig. 4).

A simplified 3D model of Fogo island (whose limits are represented in dashed red line in Fig. 4) was built considering a sharp ocean-land border (with a 4 km deep ocean) in order to study the ocean effect in

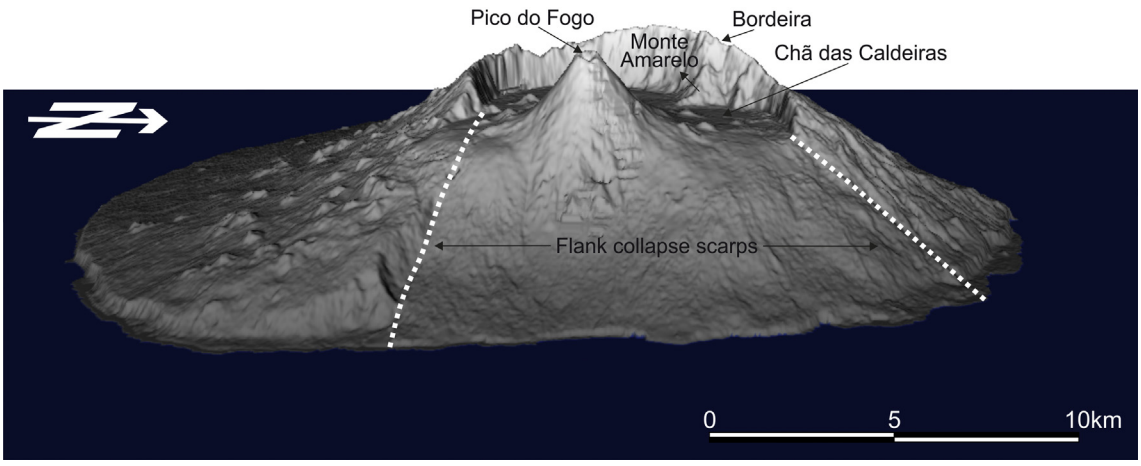

Fig. 3. Digital elevation model of the island of Fogo displaying the eastward facing depression and the flank collapse lateral scarps (highlighted with white dotted lines). The model is represented with ~2× vertical exaggeration.

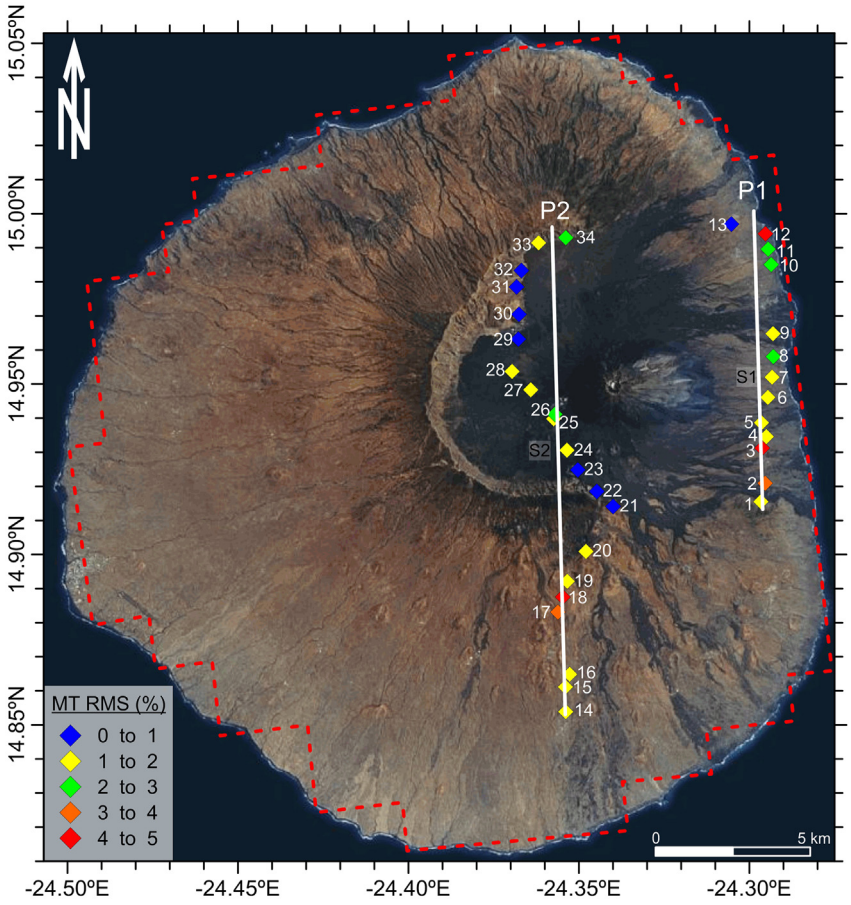

Fig. 4. Location of the MT sites corresponding to profiles 1 and 2 (P1 and P2) over an ortophoto image of Fogo. The red dashed line indicates the limits for the simplified 3D model of island of Fogo used in the investigation of the ocean effect. The MT sites used for to study the ocean effects are indicated as S1 and S2 with dots in blue. Classes of RMS values are indicated for each site by a colour code (key in lower left inset). (For interpretation of the references to colour in this figure legend, the reader is referred to the web version of this article.)

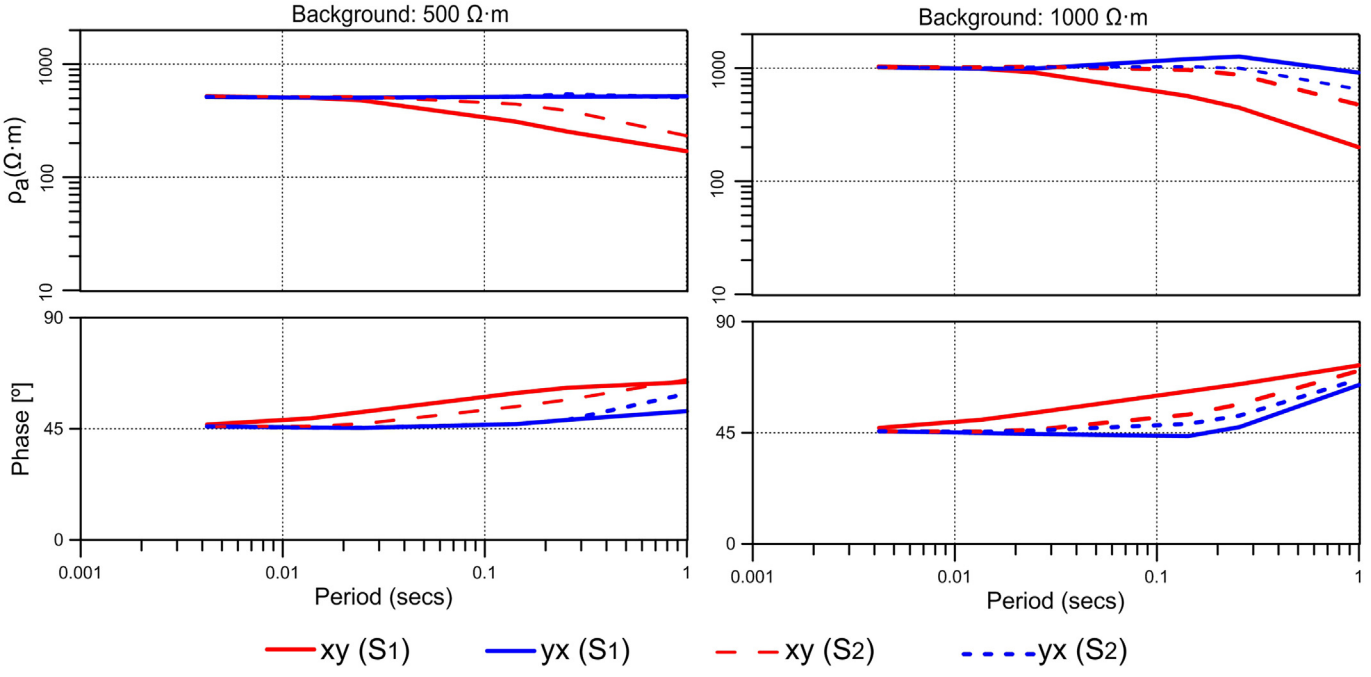

Fig. 5. Apparent resistivity and phase curves calculated from the synthetic 3D model in the period range from 0.001 to 1 s for S1 and S2 (see location in Fig. 4).

two MT sites from both profiles (indicated as S1 and S2 in Fig. 4). The island and the oceanic crust were assumed as uniform and calculations have been done with two different resistivity values: 500 and 1000 Ω·m (Ω·m). A resistivity of 0.3 Ω·m was assumed for the ocean. The forward modelling was carried out using the code developed by Mackie and Madden (1993).

Fig. 5 shows the apparent resistivity and phase curves calculated in the period range from 0.001 to 1 s at the two sites. The very deep ocean affects the xy component more than the yx one and it influences the phase curves at shorter periods. As expected, the ocean effects are stronger when the island resistivity is 1000 Ω·m. These results show that for the more realistic background resistivity of 500 Ω·m the yx data until approximately 0.1 s are not affected by the sea, even for S1 (closer to the sea), as well as the xy data in the case of site S2.

To estimate a regional strike and investigate possible distortions the Smith's (1995), decomposition method was applied at each individual sites from profile 2 (Fig. 6) considering periods from 0.001 s to 0.1 s – those not affected by the sea–. The individual strikes range from N225°E to N315°E. Accordingly, an E-W strike direction on average was selected. Thus, we proceeded with a 2D inversion but using only the TE mode (yx curves) that is less affected by the sea and considering periods until 1 s. A 2D inversion of mode TE was also carried out for profile 1 assuming the same strike as in profile 2.

The depth of resolution (DOI) has been calculated to determine the quality of the obtained profiles. For this purpose, we used the depth of investigation as defined by Oldenburg and Li (1999) and modified by Marescot et al. (2003). Determining the DOI implies to carry out two inversions of the data using different resistivities for the initial model. In this case, we used 100 and 1000 Ω·m for the first and second initial models respectively. The normalized DOI index is calculated by the formula below (Robert et al., 2011):

$$R(x,z) = \frac{m_1(x,z) - m_2(x,z)}{R_{max}\,(m_{1r} - m_{2r})}$$

where m_{1r} and m_{2r} are the resistivities of the first and second reference models, and *m1* (x,z) and *m2* (x,z) are the resistivity of each cell of these models. The DOI index (R) will approach zero where the two inversions produce the same resistivity values, regardless of the value of the reference model. For the normalized DOI index, Marescot et al. (2003) recommended a cut-off value of 0.1 or 0.2. In our case, we used the more restrictive 0.1 cut-off value.

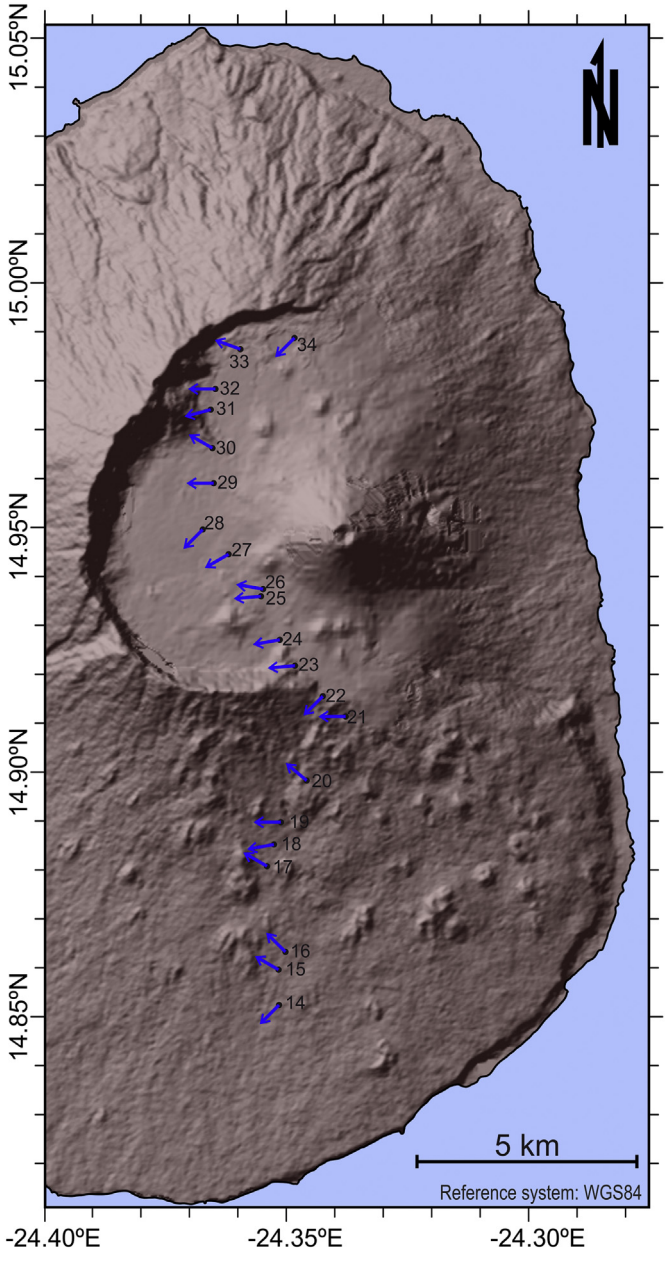

Fig. 6. Estimated strike for each individual sites. The selected sites represent the ocean effect for each profile at its midpoint.

4. 2D inversion of data

The TE mode data from both profiles was inverted assuming a 2-D model and using the Mackie's program (Mackie et al., 1997), which solves for the resistivity distribution and for static shift effect at each site. The data and model responses at some selected sites are shown in Fig. 7, where it is observed that the data misfit is in general lower than 2% (Fig. 4). The error floor used in the inversion was 5% for apparent resistivity and 5% for phases on average.

Profile 1 (Fig. 8a) highlights a low resistivity area (<5 Ω·m) embedded in a resistivity of about 100 Ω·m. The low resistive body towards the S extends for about 400 m and has a thickness of ~500 m. From metre 400 to the northern of the profile there is an extended low resistive area with a thickness of 500–600 m and an irregular base. A dashed red line at 400 m length marks the southern limit of the flank collapse according to geomorphological criteria.

Profile 2 (Fig. 8b) presents three low resistivity areas separated by zones with intermediate resistivity values of ~100 Ω·m. The southern low resistive zone, centred at about metre 4400, has short lateral extension and presents very low resistivity values of ~2 Ω·m. Further N, between metres 7600 and 13,200, a second non-homogeneous low resistive body has a horizontal extension of about 5600 m and its top is located at a depth of 700 m in the S rising to a depth of 400 m towards the N. It has a thickness of ~500 m and a resistivity lower than 10 Ω·m on average. The northernmost low resistivity region extends from metre 15,700 to the northern end of the profile presenting resistivity values of about 10 Ω·m. Its top is located at a depth of ~350 m, presents a thickness of ~500 m, and the base is slightly deeper than that of the central low resistivity body. The southern low-resistivity body lies outside the summit depression, while the central and northern bodies are located inside the summit depression and correspond to the southern and northern calderas respectively (the red dashed lines mark the places where the profile crosses the collapse caldera ring faults) according to the interpretation of Brum da Silveira et al. (1997) and Torres et al. (1998). The two zones are separated by a resistive area with values of ~180 Ω·m that corresponds to the stations located across the older basement of Monte Amarelo spur (Figs. 3 and 4). Above the two low resistivity bodies located inside the calderas there is a shallow high resistive layer with values ranging from 200 to 500 Ω·m.

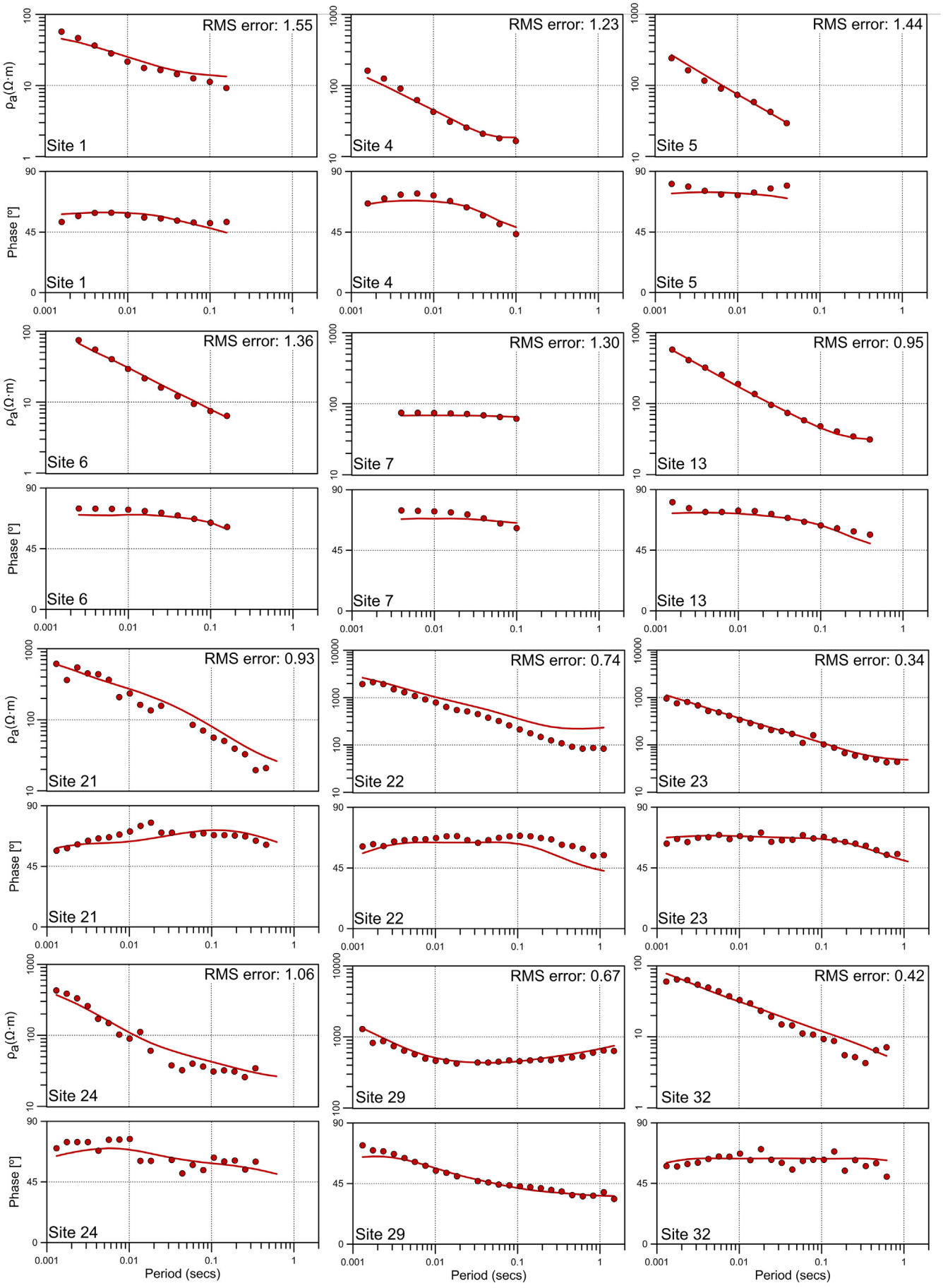

Fig. 7. Measured apparent resistivity and phase curves. The sites correspond to profile 1 (sites 1–13) and profile 2 (sites 14–34).

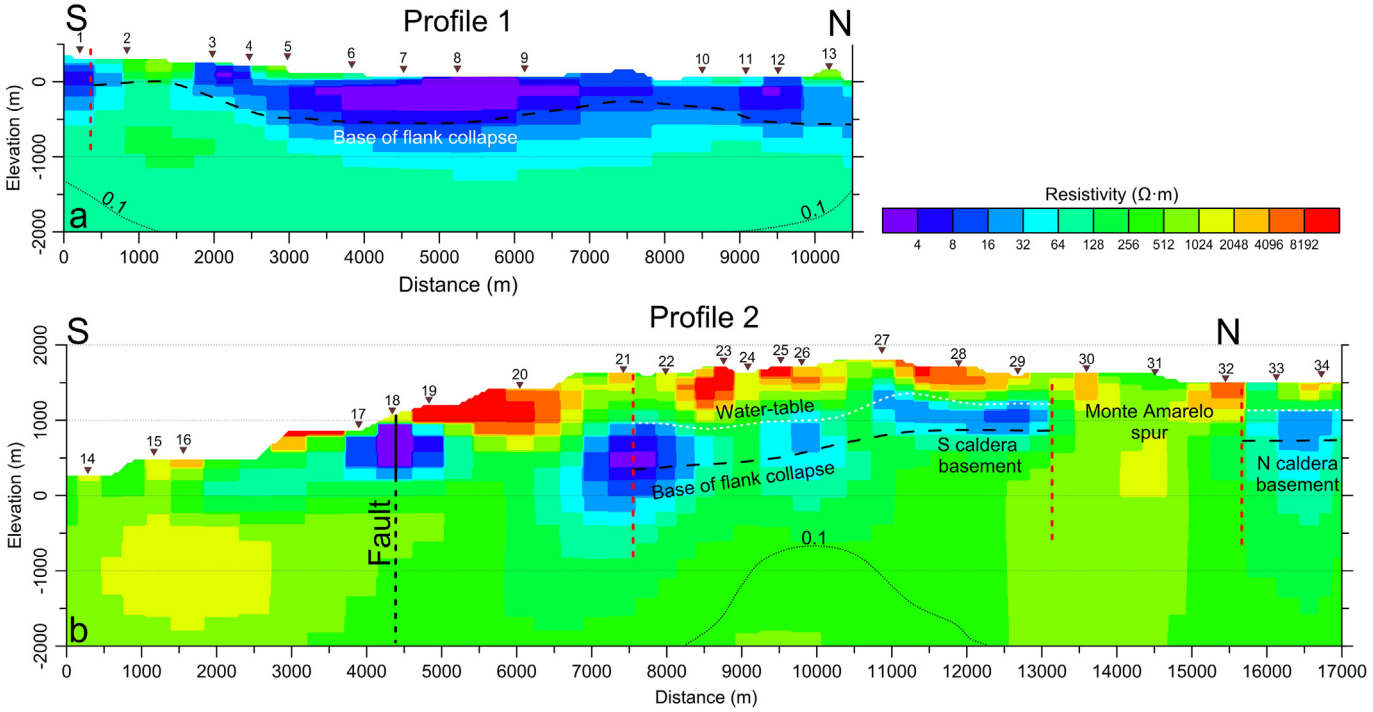

Fig. 8. Magnetotelluric profiles across Fogo collapse structures. The locations of (a) Profile 1 (coastal area) and (b) Profile 2 (summit depression) are marked in Fig. 4. Red dashed line in P1 indicates the location of the southern lateral fault of the flank collapse; in P2, the black vertical line marks the position of the fault (see Fig. 2), and the red dashed lines correspond to the location of the calderas ring faults. White dotted lines and black dashed lines mark the water table (top) and the base of the low-resistivity bodies in both profiles. The 0.1 dashed lines at the bottom indicate the depth of investigation. (For interpretation of the references to colour in this figure legend, the reader is referred to the web version of this article.)

The depth of resolution was calculated for both profiles. As marked in Fig. 8, the cut-off value of 0.1 is at the bottom of the profiles, conferring to our MT model a reliable resolution for the definition of the structures pertinent for this study.

5. Interpretation and discussion

The magnetotelluric profiles (Fig. 8) present a good correlation with the geomorphological features of the referred Fogo's collapse structures. In general, the low resistivity areas are interpreted as corresponding to the water saturated portions of the recent lava flow infill of the caldera depressions. Young lava flows are usually highly fractured and present a significant number of cavities (lava tubes and gas blisters) making them highly permeable so that its resistivity is very low when saturated. With increasing age, the permeability of lava flow sequences progressively decreases because of weathering and filling of fractures with clay minerals. Thus, the older pre-collapse lava sequences are expected to present lower permeability and consequently higher resistivity.

In profile 1 the northern low resistivity body observed between meter 1500 and 9500 represents the recent lava flow infill inside the collapsed area and defines the irregular basement and depth of the flank collapse (Fig. 3 and 8a). The low resistivity body at the S indicates the southern limit of the flank collapse and the associated fracture zone, which may have allowed seawater intrusion. The slightly higher resistivity body immediately to the north of the collapse scarp may represent a detached block of the older basement. In profile 2 (Fig. 8b), the southern low resistivity area at ~4400 m length coincides with a NNW-SSE fracture zone marked by the alignment of several young (pre-settlement) scoria cones and belonging to the N-S trending Sambango-Monte Vermelho fault system (see Fig. 2) inferred by Brum da Silveira et al. (1997) and Torres et al. (1998). The other two low resistivity bodies lie inside the southern (meter 7600 to 13,200) and northern (meter 15,750 to 17,000) collapse calderas proposed by Brum da Silveira et al. (1997). These are separated by a higher resistivity sector that corresponds to the Monte Amarelo spur, where older lava sequences are exposed or at shallow depths.

The southern lateral limit of the flank collapse is clear in profile 1 (Fig. 8a) where low resistivity area is found. This coincides with the location of the flank collapse lateral limits previously recognized in the geomorphology of Fogo eastern flank (Brum da Silveira et al., 1997; Torres et al., 1998; Day et al., 1999). The high resistivity shallow layer above recognized under some MT sites is interpreted as the unsaturated or dry upper part of the young lava sequence. At the base of the profile, the higher resistivity is interpreted as corresponding to the lower permeability pre-collapse lava sequences, probably capped by the landslide breccia. The slightly irregular base of the low resistivity body, located at an average depth of 700 m, is thus interpreted as the basal surface of the flank collapse.

The interpretation of profile 2 (Fig. 8b) is less straightforward. As in profile 1, the resistivity associated to the non-saturated recent lavas is higher (300–1000 Ω·m) than that of older ones (~100–200 Ω·m). The southern low resistivity body (~1 Ω·m), occurring in the vicinity of meter 4500, correlates with the previous mentioned NNW-SSE trending fault zone and its short lateral extension can be interpreted as corresponding to the limited width of the more permeable fractured fault zone. The very low resistivity values can only be attributed to hydrothermal fluids circulating along the fault zone.

From metre 7600 to the N, the MT stations (sites 21–34, Figs. 4 and 8b) are located inside the summit depression. A marked lateral resistivity change is observed at this location represented by very low resistivity area that can only be explained by hydrothermal fluids circulating along the fractured area of a caldera ring fault. Below the central and northern low resistivity bodies, higher resistivity sequences correspond to less permeable rocks. The central low resistivity area shows that the water-table is located at a depth of ~700 m at the S becoming shallower to the N. At metre 11,000 the water table becomes horizontal at a depth of ~350 m. We interpret the base of the aquifer as representing the basal collapse surface. Indeed, the basal surfaces of landslides are usually covered by impermeable cataclasites produced by intense shearing/

fracturing at the base of the sliding rock mass. The overlying post-flank collapse lava sequences forms a highly permeable body that presents a contrasting low resistivity. At the southern entry of the summit depression (meter 7500) the base of the aquifer is inferred to stand at an approximate depth of 1200 m progressively becoming shallower to the N to depths of around 800–900 m (e.g. meter 12,500).

The horizontal sector of the central low resistivity body (meter 11,000 to 13,150) is interpreted as corresponding to a perched aquifer within the southern caldera-filling lava sequence. Its horizontal base should correspond to the caldera bottom where post-caldera lava sequences must overlie hydrothermalized impermeable rocks. The resistive area separating the central and northern low resistivity bodies matches the sector of the profile crossing the Monte Amarelo spur (Figs. 3 and 4), thus corresponding to lower-permeability pre-caldera collapse lava sequences. Profile 2 also suggests that the base of the northern low resistivity body (meter 15,750 to 18,000) located inside the northern caldera, is slightly deeper than its southern counterpart, which is in accordance with the geomorphological step of ~50 m between the two calderas separated by the Monte Amarelo spur.

5.1. Structure of the collapse area

The well-defined limits of the low resistivity bodies observed in the MT profiles, coinciding with fractures bounding the caldera and flank collapses, support the previous geomorphological interpretation of the collapsed areas. The southern lateral limit of the flank collapse (Fig. 9a) in the coastal area is clear in profile 1. However, the northern lateral one was not reached by profile 1 but is well defined by Brum da Silveira et al. (1997; black dashed line) and Day et al. (1999; white dashed line) following geomorphological criteria. In profile 2 the area where the low resistivity bodies become horizontal agrees with the hypothesis of pre-flank collapse calderas as previously proposed by Brum da Silveira et al. (1997) and does not support the model proposed by Day et al. (1999) and Amelung and Day (2002) which considers the Bordeira as the headwall of the flank collapse. In fact, Fogo volcano lacks well-defined shallow reservoirs as deduced from geodetical and petrological studies of the latest eruptions (Amelung and Day, 2002; Hildner et al., 2011, 2012; González et al., 2015; Mata et al., 2017). However, the destruction of the magmatic feeder system and shallow reservoirs in a volcano can be explained both by large landslides and by caldera collapses, so that argument does not exclude the caldera hypothesis as proposed by Amelung and Day (2001). Therefore, the collapse limits inside Chã das Caldeiras match the 2 calderas model proposed by Brum da Silveira et al. (1997). The origin of Las Cañadas summit depression (Tenerife), which presents similar structures, has also been a case of debate. Magnetotelluric studies (Pous et al., 2002; Coppo et al., 2008; Piña-Varas et al., 2015) revealed the existence of closed depressions defining summit calderas and confirming its vertical collapse origin (Martí et al., 1994).

The limits of the flank collapse correspond to an onshore area of about 81.2 km^2. Considering that the basal plane of the flank collapse intersects the island flank below sea-level, the area of the flank collapse is slightly larger. Since there is not a detailed bathymetry of the submarine flank of the volcano we used the isobaths presented by Masson et al. (2008), which allowed us to estimate a total area of ~100 km^2 corresponding to an area increase in the order of 25%. As discussed in previous works, the Fogo landslide involved a considerable volume. Day et al. (1999) estimate the displaced volume in 150–200 km^3, while Madeira et al. (2008) proposed a more conservative estimate of the displaced volume of 70 km^3 based on the multibeam survey presented by Masson et al. (2008). This difference mainly results from the different interpretations of the nature of the summit depression. However, none of these estimates had a good constrain on the collapse depth. Considering the area of the flank collapse presented above and an average depth of ~1100 m for its basal surface we can estimate a more precise volume for the flank collapse. Note that the height of the south lateral collapse scarp (400 m) in conjunction with an average thickness of 700 m for the post-collapse lava infill agrees with the proposed thickness. Altogether, the data obtained in this work suggests a displaced volume of ~110 km^3, a value that falls between the more conservative value proposed by Madeira et al. (2008) and the larger estimates by Day et al. (1999), which result from the different interpretations of the nature of the summit depression. This value is close to those used by Paris et al. (2011) to produce the 7 scenarios of the tsunami simulations (121–124 km^3).

Fig. 9b shows an interpretative profile based on geophysical data and geological observations. This profile depicts the collapse geometry at depth based on the thickness of the recent lava sequences as suggested by the geological interpretation of the two MT profiles.

The data here presented is also important for assessing groundwater resources both in Chã das Caldeiras, where a local perched aquifer occurs within the post-calderas filling volcanic sequence, and in the eastern coastal area where the very low resistivity values indicates saltwater intrusion. Furthermore, the southern low resistivity body in profile 2

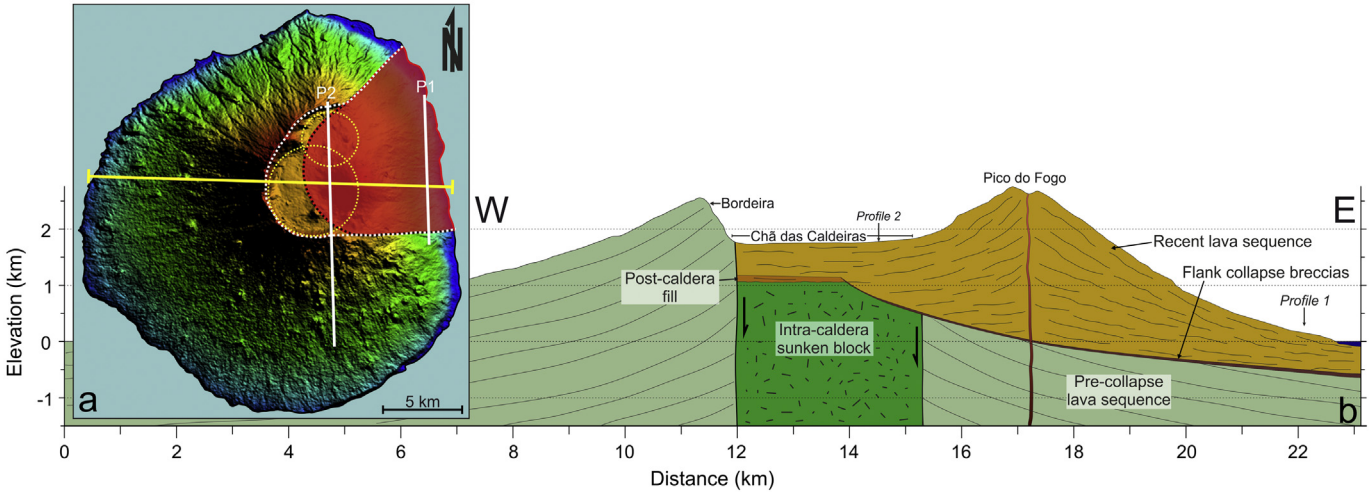

Fig. 9. Proposed interpretation for the collapse structures in Fogo. (a) Comparison between the collapse contours proposed by Day et al. (1999; dotted white line) and Madeira et al. (2008; dotted black line). The red zone indicates the area used in this study to estimate the volume of the collapse. (b) Interpretative geological profile based on the magnetotelluric profiles and geological observations. (For interpretation of the references to colour in this figure legend, the reader is referred to the web version of this article.)

constitutes additional evidence for the presence of the N-S Sambango-Monte Vermelho fault system proposed by Brum da Silveira et al. (1997).

6. Conclusions

Two approximately N-S trending magnetotelluric profiles have been obtained in the collapsed area of the island of Fogo. These profiles display low resistivity zones inside the collapse area in contact with higher resistivity bodies. These low resistivity bodies are interpreted as water saturated lava sequences corresponding to the recent very permeable caldera and flank collapse lava sequences infill, in contact with less permeable pre-collapse lavas. These highly permeable rocks allow saltwater intrusion at the coastal area (P1) and the presence of a freshwater perched aquifer inside the summit depression (P2). When considering the two competing models for the Fogo depression, the indications given by the MT profiles on the subsurface structure allow making the following interpretations. If the headwall of the flank collapse would be the Bordeira wall, then the basement beneath the post-collapse filling sequence would dip steeply to the East. Consequently, the young lavas filling the depression, standing on this surface, would not be horizontal. On the other hand, the hypothesis of two intersecting calderas justifies the presence of Monte Amarelo spur and the difference in elevation between the summit depression to the north and south of the spur (with the topographic step aligned with the spur). This 50 to 60 m difference, still observed in the present topography, is also suggested by profile 2 (Fig. 8b), with the top and base of the low resistivity body significantly lower to the north of the spur. Additionally, the young lava sequence, filling closed depressions such as the two volcanic calderas, would be horizontal matching the structure suggested by the low resistivity bodies inside the summit depression.

The MT data allowed detailing the depth of Fogo's flank collapse that produced a megatsunami ~73 ky ago. The MT data contributed to define the basement of the recent lava flow infill that, in conjunction with the lateral limits defined by geomorphological evidences (Brum da Silveira et al., 1997; Day et al., 1999), allows estimating a more precise value for the volume (110 km^3) and area (~100 km^2) of the flank collapse. The obtained MT data and its interpretation allow constraining the latest stages of the geomorphic evolution of the Fogo Island involving two distinct caldera collapses and a later (~73 ky ago) lateral flank collapse, as proposed by Brum da Silveira et al. (1997), as the preferred model. It does not endorse the model proposed by Day et al. (1999) which considers the Bordeira as the headwall of the flank collapse.

Further detail on the sub-surface structure of the collapsed area would benefit from additional magnetotelluric profiles, notably along the E-W direction inside the summit depression. However, a continuous E-W profile extending from the Bordeira wall to the eastern coast is impracticable because of the rough and steep topography and the absence of roads and paths.

This study demonstrates that magnetotelluric data is capable of accurately defining the limits of flank collapses at depth, thus being a reliable geophysical tool in the investigation of volcanic islands evolution.

Acknowledgements

The magnetotelluric survey was obtained in the scope of a contract between IDL and GESTO Energy Consulting. The authors acknowledge GESTO for the permission to use the data in this study. Geological field observations and mapping were performed in the scope of the projects INTERGEOFOGOS (POCTI/CTA/35614/99) PLINT (POCTI/CTA/45802/2002) and FIRE (PTDC/GEO-GEO/1123/2014) funded by the Portuguese research agency Fundação para a Ciência e Tecnologia (FCT). This Publication was also supported by FCT project UID/GEO/50019/2013 – Instituto Dom Luiz. We appreciate the contributions from three anonymous reviewers and the editor, Professor Jurgen Neuberg.

References

Acocella, V., Tibaldi, A., 2005. Dike propagation driven by volcano collapse: a general model tested at Stromboli, Italy. Geophys. Res. Lett. 32 (8).
Amelung, F., Day, S., 2002. InSAR observations of the 1995 Fogo, Cape Verde, eruption: implications for the effects of collapse events upon island volcanoes. Geophys. Res. Lett. 29 (12).
Ancochea, E., Huertas, M.J., Hernán, F., Brändle, J.L., 2010. Volcanic evolution of São Vicente, Cape Verde Islands: the Praia Grande landslide. J. Volcanol. Geotherm. Res. 198 (1–2), 143–157.
Ancochea, E., Huertas, M.J., Hernán, F., Brändle, J.L., 2014. A new felsic cone-sheet swarm in the Central Atlantic Islands: the cone-sheet swarm of Boa Vista (Cape Verde). J. Volcanol. Geotherm. Res. 274, 1–15.
Ancochea, E., Huertas, M.J., Hernán, F., Brändle, J.L., Alonso, M., 2015. Structure, composition and age of the small islands of Santa Luzia, Branco and Raso (Cape Verde Archipelago). J. Volcanol. Geotherm. Res. 302, 257–272.
Bagnardi, M., González, P.J., Hooper, A., 2016. High-resolution digital elevation model from tri-stereo Pleiades-1 satellite imagery for lava flow volume estimates at Fogo Volcano. Geophys. Res. Lett. 43 (12), 6267–6275.
Brum da Silveira, A., Madeira, J., Serralheiro, A., 1997. A estrutura da ilha do Fogo, Cabo Verde. A erupção vulcânica de 1995 na ilha do Fogo, Cabo Verde. Instituto de Investigação Científica Tropical e Ministério da Ciência e Tecnologia, pp. 63–78.
Cappello, A., Ganci, G., Calvari, S., Pérez, N.M., Hernández, P.A., Silva, S.V., Cabral, J., Del Negro, C., 2016. Lava flow hazard modeling during the 2014–2015 Fogo eruption, Cape Verde. J. Geophys. Res. Solid Earth 121 (4), 2290–2303.
Carracedo, J.C., 2014. Structural collapses in the Canary Islands. In: Gutiérrez, F., Gutiérrez, M. (Eds.), Landscapes and Landforms of Spain. Springer Netherlands, Dordrecht, pp. 289–306.
Coombs, M.L., Clague, D.A., Moore, G.F., Cousens, B.L., 2004. Growth and collapse of Waianae Volcano, Hawaii, as revealed by exploration of its submarine flanks. Geochem. Geophys. Geosyst. 5 (8).
Coppo, N., Schnegg, P.-A., Heise, W., Falco, P., Costa, R., 2008. Multiple caldera collapses inferred from the shallow electrical resistivity signature of the Las Cañadas caldera, Tenerife, Canary Islands. J. Volcanol. Geotherm. Res. 170 (3), 153–166.
Cortés, A., Macías, J., Capra, L., Garduño-Monroy, V., 2010. Sector collapse of the SW flank of Volcán de Colima, México: the 3600 yr BP La Lumbre–Los Ganchos debris avalanche and associated debris flows. J. Volcanol. Geotherm. Res. 197 (1), 52–66.
Day, S., 1996. Hydrothermal pore fluid pressure and the stability of porous, permeable volcanoes. Geol. Soc. Lond., Spec. Publ. 110 (1), 77–93.
Day, S., 2001. Cumbre Vieja Volcano–Potential collapse and tsunami at La Palma, Canary Islands. Geophys. Res. Lett. 28 (17), 3397–3400.
Day, S.J., Heleno da Silva, S.I.N., Fonseca, J.F.B.D., 1999. A past giant lateral collapse and present-day flank instability of Fogo, Cape Verde Islands. J. Volcanol. Geotherm. Res. 94 (1), 191–218.
Day, S., Llanes, P., Silver, E., Hoffmann, G., Ward, S., Driscoll, N., 2015. Submarine landslide deposits of the historical lateral collapse of Ritter Island, Papua New Guinea. Mar. Pet. Geol. 67, 419–438.
De Silva, S.L., Francis, P.W., 1991. Volcanoes of the Central Andes. Springer, New York.
Della Seta, M., Martino, S., Mugnozza, G.S., 2013. Quaternary sea-level change and slope instability in coastal areas: insights from the Vasto Landslide (Adriatic coast, central Italy). Geomorphology 201, 462–478.
Duprat, H.I., Friis, J., Holm, P.M., Grandvuinet, T., Sørensen, R.V., 2007. The volcanic and geochemical development of São Nicolau, Cape Verde Islands: constraints from field and 40Ar/39Ar evidence. J. Volcanol. Geotherm. Res. 162 (1–2), 1–19.
Dyhr, C.T., Holm, P.M., 2010. A volcanological and geochemical investigation of Boa Vista, Cape Verde Islands; 40Ar/39Ar geochronology and field constraints. J. Volcanol. Geotherm. Res. 189 (1–2), 19–32.
Ferrer, M., Seisdedos, J., González de Vallejo, L.I., et al., 2010. The role of hyaloclastite rocks in the stability of the volcanic island flank of Tenerife. In: Ollala (Ed.), Volcanic Rock Mechanics. Taylor and Francis, London, pp. 167–170.
González, P.J., Bagnardi, M., Hooper, A.J., Larsen, Y., Marinkovic, P., Samsonov, S.V., Wright, T.J., 2015. The 2014–2015 eruption of Fogo volcano: geodetic modeling of Sentinel-1 TOPS interferometry. Geophys. Res. Lett. 42 (21), 9239–9246.
González-Castillo, L., Junge, A., Galindo-Zaldívar, J., Löwer, A., 2015. Influence of a narrow strait connecting a large ocean and a small sea on magnetotelluric data: Gibraltar Strait. J. Appl. Geophys. 122, 103–110.
Hildner, E., Klügel, A., Hauff, F., 2011. Magma storage and ascent during the 1995 eruption of Fogo, Cape Verde Archipelago. Contrib. Mineral. Petrol. 162 (4), 751.
Hildner, E., Klügel, A., Hansteen, T.H., 2012. Barometry of lavas from the 1951 eruption of Fogo, Cape Verde Islands: implications for historic and prehistoric magma plumbing systems. J. Volcanol. Geotherm. Res. 217-218, 73–90.
Hoernle, K., Tilton, G., Le Bas, M.J., Duggen, S., Garbe-Schönberg, D., 2002. Geochemistry of oceanic carbonatites compared with continental carbonatites: mantle recycling of oceanic crustal carbonate. Contrib. Mineral. Petrol. 142 (5), 520–542.
Holm, P.M., Grandvuinet, T., Friis, J., Wilson, J.R., Barker, A.K., Plesner, S., 2008. An 40Ar-39Ar study of the Cape Verde hot spot: temporal evolution in a semistationary plate environment. J. Geophys. Res. Solid Earth 113 (B8).
Le Bas, T.P., Masson, D.G., Holtom, R.T., Grevemeyer, I., 2007. Slope failures of the flanks of the southern Cape Verde Islands. In: Lykousis, V., Sakellariou, D., Locat, J. (Eds.), Submarine Mass Movements and their Consequences: 3 International Symposium. Springer, Netherlands, Dordrecht, pp. 337–345.
Lee, H.J., 2009. Timing of occurrence of large submarine landslides on the Atlantic Ocean margin. Mar. Geol. 264 (1), 53–64.
López, D.L., Williams, S.N., 1993. Catastrophic volcanic collapse: relation to hydrothermal processes. Science 260 (5115), 1794–1796.

Maccaferri, F., Richter, N., Walter, T.R., 2017. The effect of giant lateral collapses on magma pathways and the location of volcanism. Nat. Commun. 8 (1), 1097.
Mackie, R.L., Madden, T.R., 1993. Conjugate direction relaxation solutions for 3-D magnetotelluric modeling. Geophysics 58 (7), 1052–1057.
Mackie, R., Rieven, S., Rodi, W., 1997. User's manual and software documentation for two-dimensional inversion of magnetotelluric data. GEOTOOLS user's guide RLM2DI supplement.
Madeira, J., Brum da Silveira, A., Mata, J., Mourão, C., Martins, S., 2008. The role of mass movements on the geomorphologic evolution of island volcanoes: examples from Fogo and Brava in the Cape Verde archipelago. Comunicações Geológicas 95, 93–106.
Madeira, J., Mata, J., Mourão, C., da Silveira, A.B., Martins, S., Ramalho, R., Hoffmann, D.L., 2010. Volcano-stratigraphic and structural evolution of Brava Island (Cape Verde) based on 40Ar/39Ar, U–Th and field constraints. J. Volcanol. Geotherm. Res. 196 (3), 219–235.
Marescot, L., Loke, M.H., Chapellier, D., Delaloye, R., Lambiel, C., Reynard, E., 2003. Assessing reliability of 2D resistivity imaging in mountain permafrost studies using the depth of investigation index method. Near Surface Geophys. 1 (2), 57–67.
Martí, J., Mitjavila, J., Araña, V., 1994. Stratigraphy, structure and geochronology of the Las Cañadas caldera (Tenerife, Canary Islands). Geol. Mag. 131 (6), 715–727.
Martí, J., Hurlimann, M., Ablay, G.J., Gudmundsson, A., 1997. Vertical and lateral collapses on Tenerife (Canary Islands) and other volcanic ocean islands. Geology 25 (10), 879–882.
Martínez-Moreno, F.J., Monteiro-Santos, F.A., Madeira, J., Bernardo, I., Soares, A., Esteves, M., Adão, F., 2016. Water prospection in volcanic islands by time domain electromagnetic (TDEM) surveying: the case study of the islands of Fogo and Santo Antão in Cape Verde. J. Appl. Geophys. 134, 226–234.
Masson, D., 1996. Catastrophic collapse of the flank of El Hierro about 15,000 years ago, and the history of large flank collapses in the Canary Islands. Geology 24, 231–234.
Masson, D., Watts, A., Gee, M., Urgeles, R., Mitchell, N., Le Bas, T., Canals, M., 2002. Slope failures on the flanks of the western Canary Islands. Earth Sci. Rev. 57, 1): 1–35.
Masson, D., Le Bas, T., Grevemeyer, I., Weinrebe, W., 2008. Flank collapse and large-scale landsliding in the Cape Verde Islands, off West Africa. Geochem. Geophys. Geosyst. 9 (7).
Mata, J., Martins, S., Mattielli, N., Madeira, J., Faria, B., Ramalho, R., Silva, P., Moreira, M., Caldeira, R., Rodrigues, J., 2017. The 2014–15 eruption and the short-term geochemical evolution of the Fogo volcano (Cape Verde): evidence for small-scale mantle heterogeneity. Lithos 288, 91–107.
McGuire, W.J., 1996. Volcano instability: a review of contemporary themes. Geol. Soc. Lond., Spec. Publ. 110 (1), 1–23.
Merle, O., Lénat, J.F., 2003. Hybrid collapse mechanism at Piton de la Fournaise volcano, Reunion Island, Indian Ocean. J. Geophys. Res. B Solid Earth 108 (3), 6–11 (ECV 6-1).
Merle, O., Barde-Cabusson, S., de Vries, B.V.W., 2010. Hydrothermal calderas. Bull. Volcanol. 72 (2), 131–147.
Mitchell, J.G., Le Bas, M.J., Zielonka, J., Furnes, H., 1983. On dating the magmatism of Maio, Cape Verde Islands. Earth Planet. Sci. Lett. 64 (1), 61–76.
Monteiro Santos, F.A., Nolasco, M., Almeida, E.P., Pous, J., 2001. Coast effects on magnetic and magnetotelluric transfer functions and their correction: application to MT soundings carried out in SW Iberia. Earth Planet. Sci. Lett. 186 (2), 283–295.
Monteiro Santos, F.A., Trota, A., Soares, A., Luzio, R., Lourenço, N., Matos, L., Almeida, E., Gaspar, J.L., Miranda, J.M., 2006. An audio-magnetotelluric investigation in Terceira Island (Azores). J. Appl. Geophys. 59 (4), 314–323.
Morgan, J.K., Moore, G.F., Clague, D.A., 2003. Slope failure and volcanic spreading along the submarine south flank of Kilauea volcano, Hawaii. J. Geophys. Res. Solid Earth 108 (B9).
Oehler, J.-F., Lénat, J.-F., Labazuy, P., 2008. Growth and collapse of the Reunion Island volcanoes. Bull. Volcanol. 70 (6), 717–742.
Okubo, C.H., 2004. Rock mass strength and slope stability of the Hilina slump, Kīlauea volcano, Hawai'i. J. Volcanol. Geotherm. Res. 138 (1), 43–76.
Oldenburg, D.W., Li, Y., 1999. Estimating depth of investigation in dc resistivity and IP surveys. Geophysics 64 (2), 403–416.
Paris, R., Giachetti, T., Chevalier, J., Guillou, H., Frank, N., 2011. Tsunami deposits in Santiago Island (Cape Verde archipelago) as possible evidence of a massive flank failure of Fogos volcano. Sediment. Geol. 239 (3–4), 129–145.
Piña-Varas, P., Ledo, J., Queralt, P., Marcuello, A., Bellmunt, F., Ogaya, X., Pérez, N., Rodriguez-Losada, J., 2015. Vertical collapse origin of Las Cañadas caldera (Tenerife, Canary Islands) revealed by 3-D magnetotelluric inversion. Geophys. Res. Lett. 42 (6), 1710–1716.
Plesner, S., Holm, P.M., Wilson, J.R., 2003. 40Ar–39Ar geochronology of Santo Antão, Cape Verde Islands. J. Volcanol. Geotherm. Res. 120 (1–2), 103–121.
Pous, J., Heise, W., Schnegg, P.-A., Muñoz, G., Martí, J., Soriano, C., 2002. Magnetotelluric study of the Las Cañadas caldera (Tenerife, Canary Islands): structural and hydrogeological implications. Earth Planet. Sci. Lett. 204 (1), 249–263.
Ramalho, R., Helffrich, G., Schmidt, D., Vance, D., 2010. Tracers of uplift and subsidence in the Cape Verde archipelago. J. Geol. Soc. 167 (3), 519–538.
Ramalho, R.S., Quartau, R., Trenhaile, A.S., Mitchell, N.C., Woodroffe, C.D., Ávila, S.P., 2013. Coastal evolution on volcanic oceanic islands: a complex interplay between volcanism, erosion, sedimentation, sea-level change and biogenic production. Earth Sci. Rev. 127, 140–170.
Ramalho, R.S., Winckler, G., Madeira, J., Helffrich, G.R., Hipólito, A., Quartau, R., Adena, K., Schaefer, J.M., 2015. Hazard potential of volcanic flank collapses raised by new megatsunami evidence. Sci. Adv. 1 (9), e1500456.
Reid, M.E., Sisson, T.W., Brien, D.L., 2001. Volcano collapse promoted by hydrothermal alteration and edifice shape, Mount Rainier, Washington. Geology 29 (9), 779–782.
Ribeiro, O., 1960. A Ilha do Fogo e as suas Erupções-Memórias. (série geográfica I), Junta de Investigação do Ultramar. 2nd Ed. (Lisboa, Portugal. 319 pp. In Portuguese, Lisboa (Portugal)).
Richter, N., Favalli, M., de Zeeuw-van Dalfsen, E., Fornaciai, A., da Silva Fernandes, R.M., Pérez, N.M., Levy, Judith, Silva Victória, S., Walter, T.R., 2016. A post-2015 lava flow hazard map for Fogo Volcano. GFZ Data Services, Cabo Verde https://doi.org/10.5880/GFZ.2.1.2016.001.
Robert, T., Dassargues, A., Brouyère, S., Kaufmann, O., Hallet, V., Nguyen, F., 2011. Assessing the contribution of electrical resistivity tomography (ERT) and self-potential (SP) methods for a water well drilling program in fractured/karstified limestones. J. Appl. Geophys. 75 (1), 42–53.
Romagnoli, C., Tibaldi, A., 1994. Volcanic Collapse in Different Tectonic Settings: An Example from the Aeolian Arc, Italy, Proceedings of International Conference on Volcano Instability on the Earth and Other Planets. The Geological Society of London.
Romagnoli, C., Kokelaar, P., Rossi, P., Sodi, A., 1993. The submarine extension of Sciara del Fuoco feature (Stromboli Island): morphologic characterization. Acta Vulcanol. 3, 91–98.
Smith, J.T., 1995. Understanding telluric distortion matrices. Geophys. J. Int. 122 (1), 219–226.
Tibaldi, A., 2001. Multiple sector collapses at Stromboli volcano, Italy: how they work. Bull. Volcanol. 63 (2–3), 112–125.
Tibaldi, A., Pasquaré, G., Francalanci, L., Gardu o, V., 1994. Collapse type and recurrence at Stromboli volcano, associated volcanic activity, and sea level changes. Atti Dei Convegni Lincei-Accademia Nazionale Dei Lincei 112, 143–152.
Torres, P.C., Madeira, J., Silva, L.C., Brum da Silveira, A., Serralheiro, A. Mota Gomes, A., 1998. Carta geológica da Ilha do Fogo (República de Cabo Verde): erupções históricas e formações enquadrantes. Geological Map Lattex, (1 sheet at 1:25.000 scale).
Torres, P., Silva, L., Serralheiro, A., Tassinari, C., Munhá, J., 2002. Enquadramento geocronológico pelo método K/Ar das principais sequências vulcano-estratigráficas da Ilha do Sal—Cabo Verde. Garcia de Orta, Série Geológica 18, 9–13.
Van Wyk de Vries, B., Kerle, N., Petley, D., 2000. Sector collapse forming at Casita volcano, Nicaragua. Geology 28 (2), 167–170.
Vezzoli, L., Corazzato, C., 2016. Volcaniclastic dykes tell on fracturing, explosive eruption and lateral collapse at Stromboli volcano (Italy). J. Volcanol. Geotherm. Res. 318, 55–72.
Voight, B., Elsworth, D., 1997. Failure of volcano slopes. Geotechnique 47 (1), 1–31.
Vozoff, K., 1991. The magnetotelluric method. Electromagnetic Methods in Applied Geophysics. Application, parts A and B. Society of exploration geophysicists Vol. 2, pp. 641–712.
Ward, S.N., Day, S., 2001. Cumbre Vieja Volcano - potential collapse and tsunami at La Palma, Canary Islands. Geophys. Res. Lett. 28 (17), 3397–3400.
Ward, S.N., Day, S., 2003. Ritter Island volcano—lateral collapse and the tsunami of 1888. Geophys. J. Int. 154 (3), 891–902.
Watts, A., Masson, D., 1995. A giant landslide on the north flank of Tenerife, Canary Islands. J. Geophys. Res. Solid Earth 100 (B12), 24487–24498.
White, R.S., 1989. Asthenospheric control on magmatism in the ocean basins. Geol. Soc. Lond., Spec. Publ. 42 (1), 17–27.